Modeling of Hermetic Transitions for Microwave Packages

Jong-Gwan Yook, Nihad I. Dib, Eray Yasan, and Linda P. B. Katehi

Radiation Laboratory, Department of Electrical Engineering and Computer Science, University of Michigan, Ann Arbor, Michigan 48109-2122

Received November 20, 1995; revised March 25, 1996.

ABSTRACT

Two numerical techniques, the finite difference in time domain (FDTD) and the finite element method (FEM) in frequency domain, are employed to characterize microstrip hermetic transition geometries in an effort to investigate high-frequency effects. Measurements performed on these transitions compare favorably with theory. Two different types of transitions have been analyzed from 10 to 25 GHz and have been found to be limited in performance by higher return loss as frequency increases. It is shown that microstrip-through-CPW hermetic transitions in the shielded environment may suffer from parasitic waveguide modes which, however, can be eliminated with the use of vias at appropriate locations. The hermetic wall on top of the CPW section shows a relatively small ($\leq$ 2 dB) effect on the original circuit performance. Similarly, the hermetic bead transition shows good performance at a lower frequency region while it degrades as frequency increases. This indicates the need for very careful characterization of transitions intended for use in microwave and millimeter-wave applications.

INTRODUCTION

Hermetic packages are frequently utilized in microwave integrated circuits to provide protection from a hostile environment in addition to reduced electromagnetic interference and radiation leakage. Although hermetic packages are designed to isolate one or more parts of the circuitry and protect them from parasitic electromagnetic noise generated by other analog or digital components, they should not affect the functionality of the packaged circuit. Despite these widely acknowledged and desired attributes of packages, the state of the art in packaging is hindered by design inefficiencies and shortcomings. As mentioned in many studies [1–15], the electrical performance of hermetic packages is not considered during the first circuit design stage and, in many cases, it turns out that the presence of the package drastically disturbs circuit characteristics. Recently, more rigorous analysis of the effect of hermetic walls and packages has been reported [16–27] and reveals a complex and vague design problem which is largely intensified by uncontrollable package interference effects on circuit performance [9].

Inevitably, the circuit in a package needs to be connected to the outer world by means of effective transitions and the performance of those transition structures needs to be carefully studied to obtain desirable overall circuit response. In most applications, a hermetic wall, which allows access to the interior of a package, is made of a perfect electric conductor (PEC) placed on top of a low dielectric constant material (ceramic). The package is placed on top of the circuit in such a way that the input and output lines are sand-

International Journal of Microwave and Millimeter-Wave Computer-Aided Engineering, Vol. 6, No. 5, 351–368 (1996)

CCC 1050-1827/96/050351-18

wiched between the ceramic and the substrate in a stripline type of configuration. The transition of the feeding line from an outside microstrip to an inside stripline through a hermetic wall locally alters the characteristics of the line, thus leading to reflections and many times localized resonance effects. There have been several studies on the effect of hermetic packages on circuit performance based on the use of an appropriate equivalent circuit which replaces the package walls. The element values of this equivalent circuit are computed through a combination of measured data and ideal transmission line theory.

A hermetic package with a coplanar waveguide type transition was used in ref. 4 to achieve input and output port insertion loss of less than 0.25 dB. In ref. 5, a microwave surface mount package was modeled as a combination of coplanar waveguide and microstrip line sections with via holes to simulate the walls and equalize ground potential. In this situation, the circuit components and transmission lines were replaced by electric equivalent circuits whose element values were extracted from measurements. For relatively high-frequency applications (up to 20 GHz) with low transmission line loss and high port-to-port isolation, a surface-mounted MIC package with plated through-holes to a microstrip transition structure has been reported [6]. Finally, in ref. 7, a 70-mil microstrip package for a high-frequency, high-power circuit application was modeled by an equivalent RLC circuit and the values of those equivalent circuit elements were determined by measurements augmented with computer calculations.

In this article, the effects of hermetic walls on the characteristics of two different types of transitions are studied. The first type is an intrachip transition, whereas the second type is an interchip transition in which the packaged circuits and connecting lines are printed on different substrates. As a result the transition geometries of the second type include finite gaps between the chips that may cause increased interference or even resonances and may substantially affect performance. The main characteristic of the first type transition is the use of a CPW configuration at the transition region. This choice is based on the

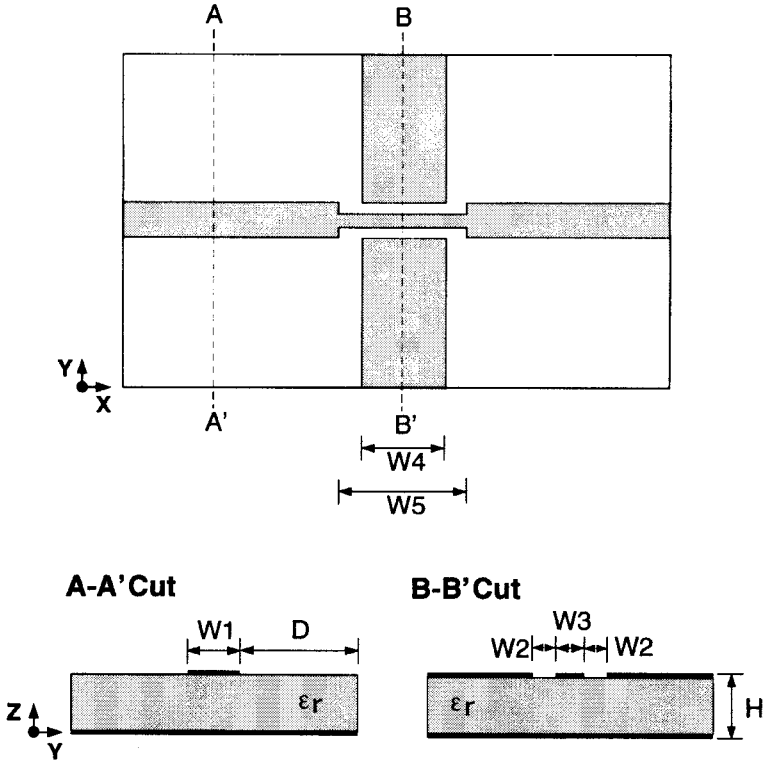

Figure 1. Geometry of the microstrip-through-CPW transition without hermetic wall. W_1 = 0.48 mm, W_2 = 0.14 mm, W_3 = 0.2 mm, W_4 = 2.0 mm, W_5 = 3.0 mm, H = 0.635 mm, ϵ_r = 12.5, Case 1: D = 2.26 mm. Case 2: D = 1.76 mm.

observation that the characteristic impedance of the microstrip line is determined mostly by the substrate thickness and conductor width, whereas that of the CPW is mainly affected by the ratio of the center conductor width to gap width. This implies that a microstrip transition is more sensitive to the surrounding environment than a transition of CPW type.

In the following, a 50-Ω-to-50-Ω microstrip-to-CPW transition is studied and the effect of the hermetic wall which is laid on top of the CPW section is investigated. As another type of hermetic transition, a hermetic bead transition structure is also analyzed. Even though the equivalent circuit approaches based on measurement data can provide an understanding of the effect of the hermetic packages on the original circuit, rigorous theoretical investigation is required for the thorough understanding of the electrical performance of these transitions. In this work, the finite element method (FEM) with edge-based vector basis function is used to characterize various types of hermetic transitions and the finite difference time domain (FDTD) method as a validation tool. The use of both techniques indicates that there is very good comparison with the exception of moderate differences at frequencies close to resonances.

FINITE ELEMENT METHOD

To determine the electromagnetic field distribution in a given space with the finite element method, one needs to solve Maxwell's equations under certain boundary conditions for a unique solution. In a simple source-free media, time harmonic electromagnetic fields satisfy the vector wave equation:

$$\nabla \times \nabla \times \mathbf{E} - k_0^2 \mu_r \epsilon_r \mathbf{E} = 0 \qquad (1)$$

where $k_0 (= \omega\sqrt{\mu_0 \epsilon_0})$ is the wavenumber in the vacuum, and μ_r and ϵ_r are relative permeability and permittivity of the medium, respectively.

As a first step toward finding the finite element solution, a given solution space, V, is subdivided into a number of small subdomains, V^e, and a weighting function, $\mathbf{Q}_j$, is defined in V^e so that:

$$\langle \mathbf{Q}_j, \nabla \times \nabla \times \mathbf{E} - k_0^2 \mu_r \epsilon_r \mathbf{E} \rangle = 0 \qquad (2)$$

where the inner product $\langle \mathbf{A}, \mathbf{B} \rangle$ is defined as:

$$\langle \mathbf{A}, \mathbf{B} \rangle = \iiint_{V^e} \mathbf{A} \cdot \mathbf{B}\, dv$$

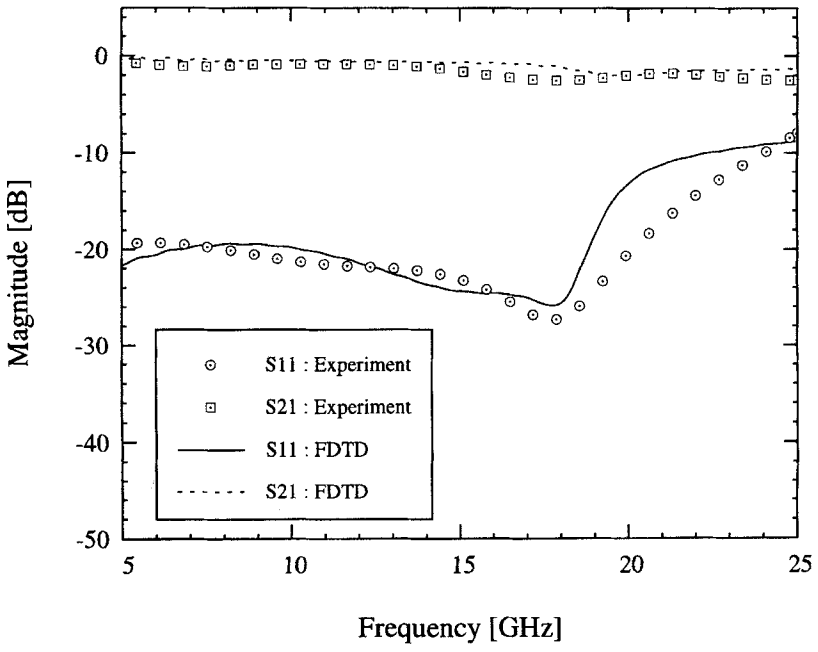

Figure 2. Computed and measured S-parameters for the transition shown in Figure 1 in an open environment. In this case, duroid substrate, which has a relate dielectric constant ϵ_r of 10.8, is used. The CPW ground planes and the PEC underneath the substrate are connected in the measurements.

With the aid of known vector identities and the divergence theorem, eq. (2) can be written as:

$$\langle(\nabla \times \mathbf{E}), (\nabla \times \mathbf{Q}_j)\rangle - k_0^2 \mu_r \epsilon_r \langle \mathbf{E}, \mathbf{Q}_j \rangle + j\omega\mu_0 \mu_r \oint_S (\mathbf{n} \times \mathbf{H}) \cdot \mathbf{Q}_j \, ds = 0 \quad (3)$$

In view of the continuity of the magnetic field across any material interface bearing no surface current, it is recognized that the contribution from the last term of eq. (3) for interior V^e is zero except for the cases in which there are sources. Moreover, on the outermost boundary, the contribution from weighting function is zero

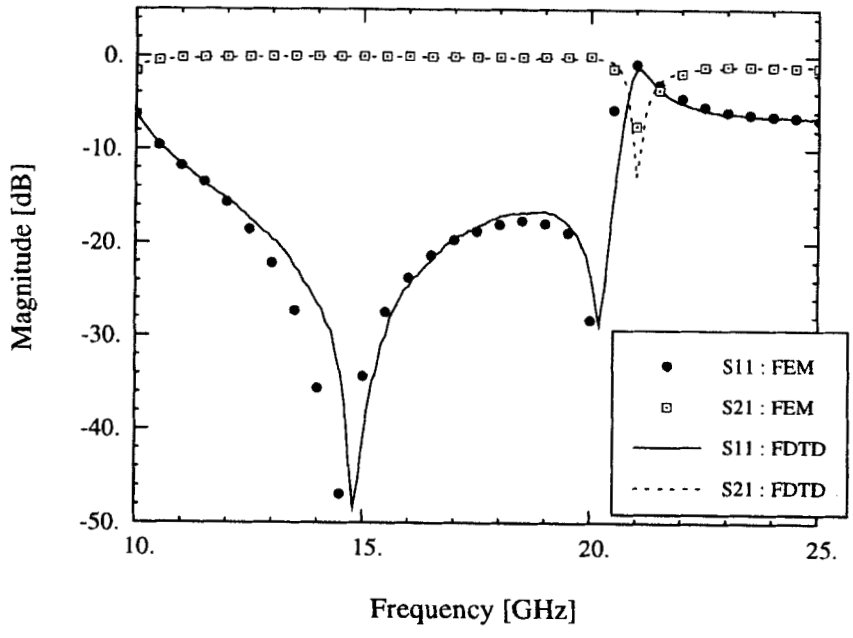

(a)

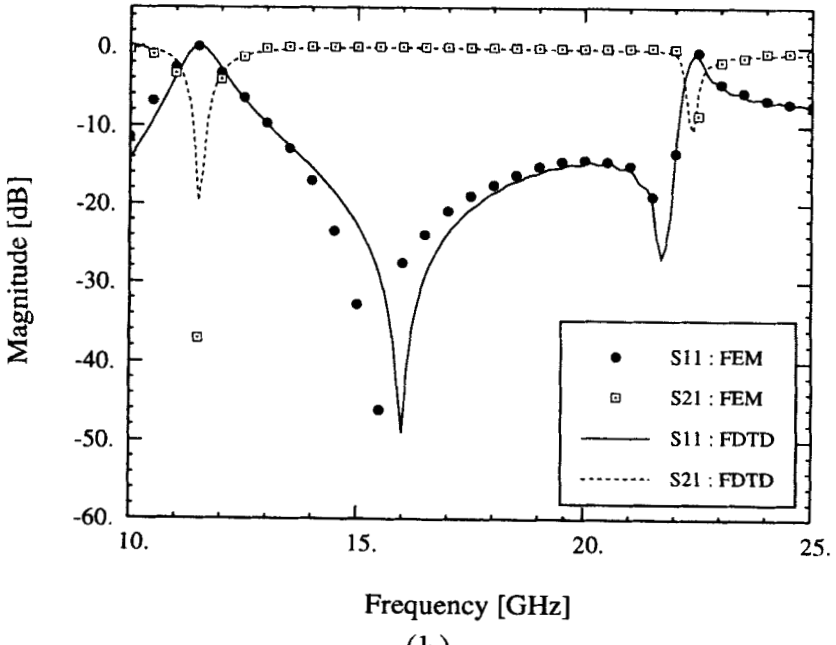

(b)

Figure 3. Comparison of FEM and FDTD data for (a) case 1 (D = 2.26 mm), and (b) case 2 (D = 1.76 mm).

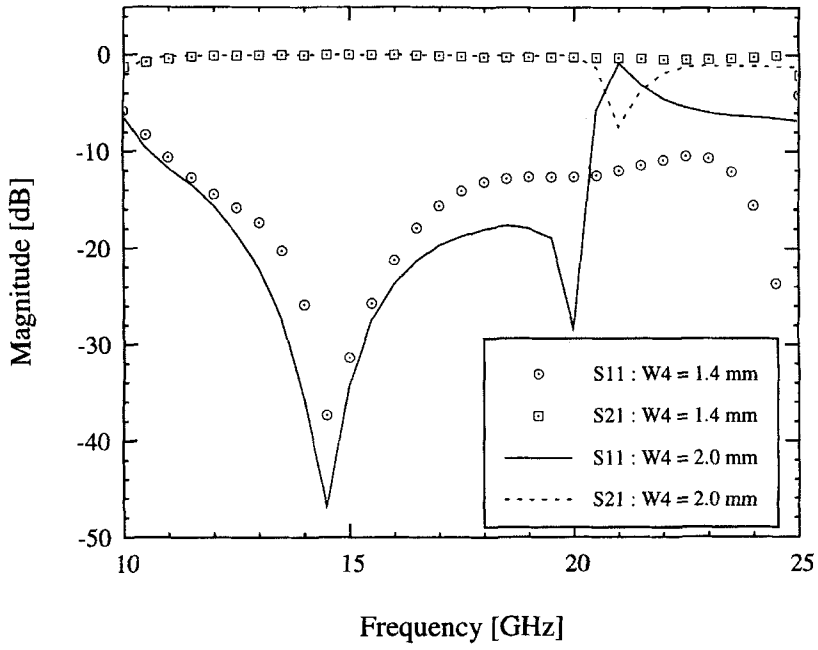

Figure 4. S-parameters for two different sizes of CPW ground plane (W_4 in Fig. 1). Other geometric factors remain the same.

on PEC surfaces and $\mathbf{n} \times \mathbf{H}$ is zero on PMC surfaces. This term, however, can be used as an ideal current source for a radiation problem.

Now, the electric field $\mathbf{E}$ in subdomain V^e can be approximated as a linear combination of known basis functions $\mathbf{P}_i$:

$$\mathbf{E} = \sum_{i=1}^{m} \alpha_i \mathbf{P}_i \tag{4}$$

where α_i values are the unknown coefficients to be determined through the solution process. By substituting eq. (4) into eq. (3), and summing up the effects of all the subdomain elements, one ends up with the following matrix equation:

$$[\mathbf{A}]T[\alpha] = [\mathbf{F}] \tag{5}$$

where:

$$A_{ij} = \langle (\nabla \times \mathbf{P}_i), (\nabla \times \mathbf{Q}_j) \rangle - k_0^2 \mu_r \epsilon_r \langle \mathbf{P}_i, \mathbf{Q}_j \rangle$$

$$F_j = -j\omega\mu_0 \mu_r \oint_S (\mathbf{n} \times \mathbf{H}) \cdot \mathbf{Q}_j \, ds$$

and $1 \leq i, j \leq N$, and N is the total number of unknowns. In this article, edge-based vector basis function, $\mathbf{W}_j^e$, with tetrahedral subdomain elements [28] are chosen as both basis and weighting

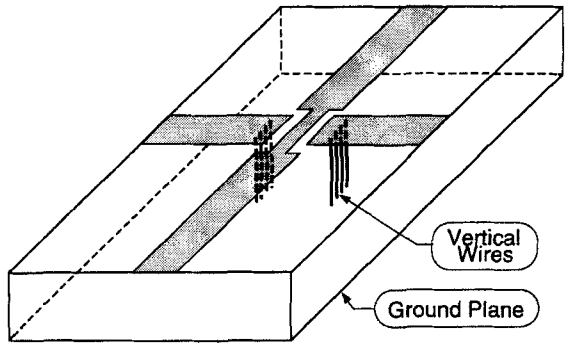

Top View (1/4 of the structure)

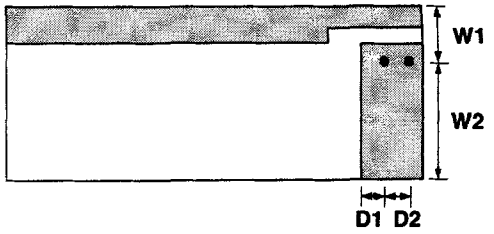

Figure 5. Geometry of the microstrip-through-CPW transition without hermetic wall: vertical wire grounding. W_1 = 0.466 mm, W_2 = 2.034 mm, D_1 = 0.40 mm, D_2 = 0.40 mm. Other geometric factors are the same as those in the previous example.

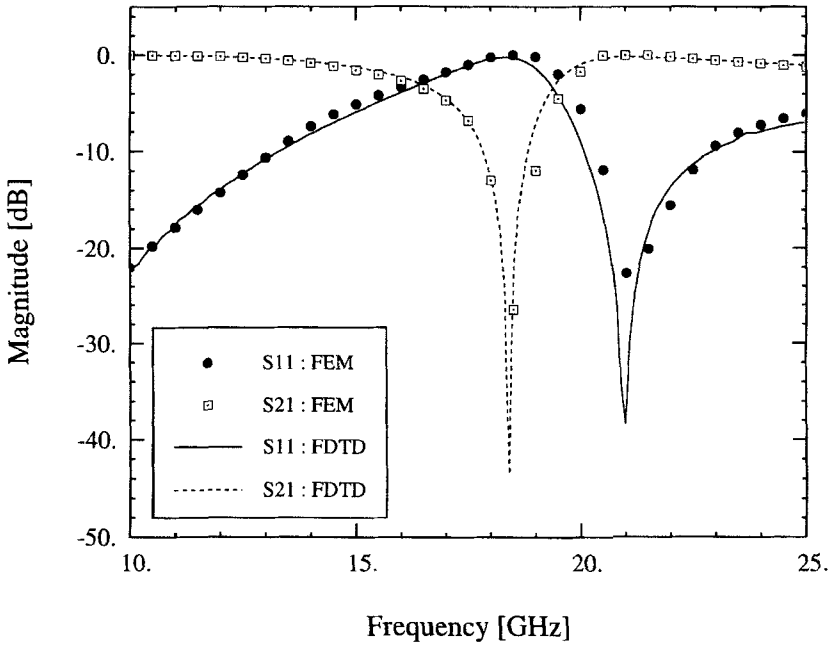

Figure 6. S-parameters of the vertical wire grounding case.

functions ($\mathbf{P}_i = \mathbf{W}_i^e$, $\mathbf{Q}_j = \mathbf{W}_j^e$). Note that $\mathbf{W}_j^e$ does enforce the tangential continuity of the $\mathbf{E}$ on a triangular surface and allows discontinuity of the normal component across the surface. The basis functions satisfy "the divergence-free condition" since the $\mathbf{E}$ field obtained from a linear combination of the basis functions exactly satisfies $\nabla \cdot \mathbf{E} = 0$. The divergence-free condition and the modeling capability of the basis functions for the null space of the curl operator contribute to the fact that the solutions are not contaminated with spurious modes [30,31], which is a serious drawback of the node-based FEM.

The final matrix equation is of very large order but the corresponding square matrix is sparse, thus allowing for the use of appropriate iterative techniques. Usually, the number of nonzero elements in a given row or column ranges from 14 to 19 for a structured mesh. In this work, the biconjugate gradient method with diagonal preconditioning has been implemented to speed up calculations and improve accuracy [32].

FINITE DIFFERENCE TIME DOMAIN METHOD

To characterize any planar discontinuity, propagation of a specific time-dependent function through the structure is simulated using the FDTD technique. The time dependence of the

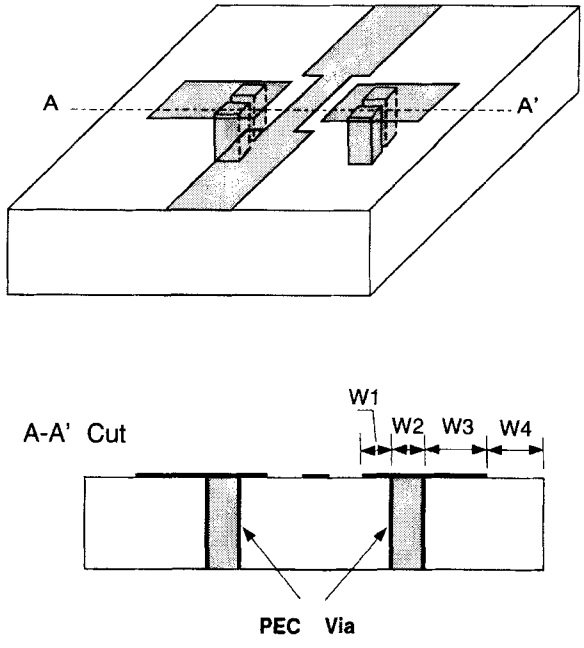

Figure 7. Geometry of the microstrip-through-CPW transition without hermetic wall: Rectangular via hole grounding with finite size CPW ground plane. The size of the via hole is 0.452 × 0.6 mm. W_1 = 0.226 mm, W_2 = 0.452 mm, W_3 = 0.452 mm, W_4 = 1.13 mm. Other geometrical factors are identical to those in the first example.

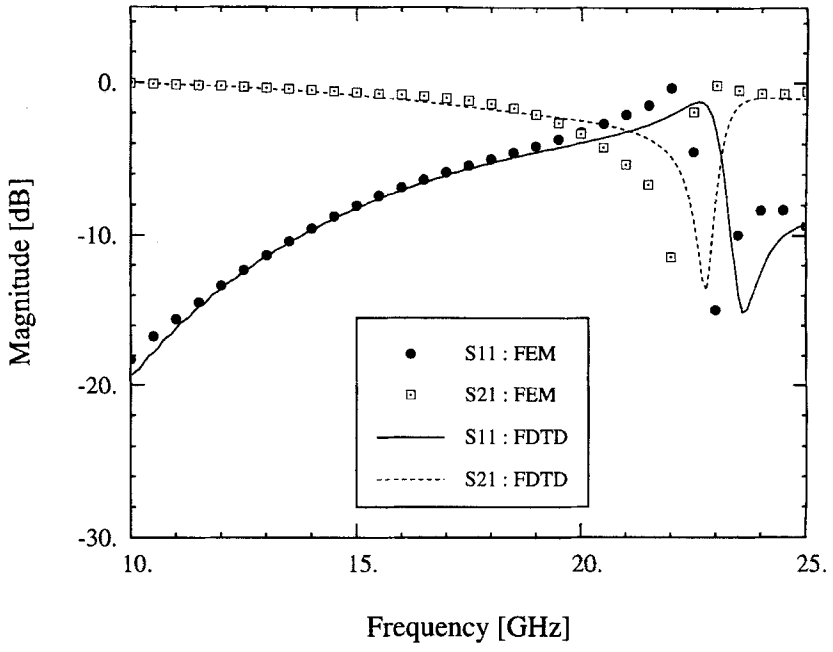

Figure 8. *S*-parameters for the rectangular via hole grounding case.

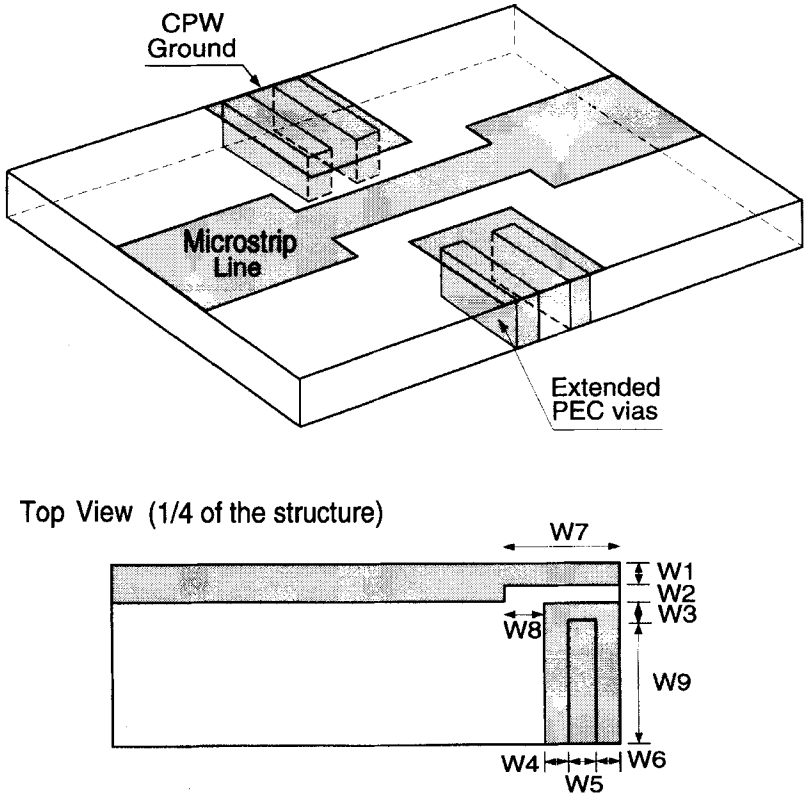

Figure 9. Geometry of the microstrip-through-CPW transition without hermetic wall: extended rectangular via hole grounding. The top view shows one quarter of the whole geometry. $W_1 = 0.1$ mm, $W_2 = 0.14$ mm, $W_3 = 0.226$ mm, $W_4 = 0.2$ mm, $W_5 = 0.6$ mm, $W_6 = 0.2$ mm, $W_7 = 1.5$ mm, $W_8 = 0.5$ mm, $W_9 = 2.034$ mm.

excitation can be chosen arbitrarily; however, a Gaussian pulse is often used because it varies smoothly in time and its Fourier transform is also a Gaussian function centered at zero frequency. Following the time and space discretizations of the electric and magnetic field components, the FDTD equivalents of Maxwell's equations are then used to update the spatial distributions of these components at alternating half-time steps [33]. The space steps, Δx, Δy, and Δz, are carefully chosen such that integral numbers of them can approximate the various dimensions of the structure. As a rule of thumb, and in order to reduce truncation and grid dispersion errors, the maximum step size is chosen to be less than 1/20 of the smallest wavelength existing in the computational domain. Then, the Courant stability criterion is used to select a time step that insures numerical stability.

In this study, the electric field component parallel to the metal strip is excited and a ground plane is placed behind the source. After the pulse has been launched, the ground plane at the front wall is switched into an absorbing boundary. Alternatively, the vertical electric field component at the front plane under the metal strip may be excited and the magnetic wall source condition [35] is used to compute the fields elsewhere in this plane. It has been found that both excitation mechanisms give the same final results.

In this article, the super-absorbing first-order Mur boundary condition is utilized to terminate the FDTD lattice at the front and back walls to simulate infinite lines. Except for one open geometry, all structures analyzed in this study are assumed to be shielded by a perfectly conducting rectangular waveguide. For this specific open structure, the first-order Mur boundary condition is used on the top and side walls to simulate an open environment.

In general, the frequency-dependent S-parameters, S_{ij}, can be obtained as follows [35]:

$$S_{ij}(\omega) = \frac{V_i(\omega)}{V_j(\omega)} \sqrt{\frac{Z_{0j}(\omega)}{Z_{0i}(\omega)}} \tag{6}$$

where V_i and V_j are the voltages at ports i and j, respectively, and Z_{0j} and Z_{0i} are the characteristic impedances of the lines connected to these ports. The voltages are obtained by taking the Fourier transform of a time record of the voltage underneath the center of the strip, which is obtained by numerically integrating the vertical electric field. To obtain $S_{11}(\omega)$, the incident and reflected fields must be known. Since the FDTD simulation calculates the total field, which is the sum of the incident and reflected waveforms, the incident field is obtained from a line of an infinite extent and is subtracted from the total waveform to yield the reflected field.

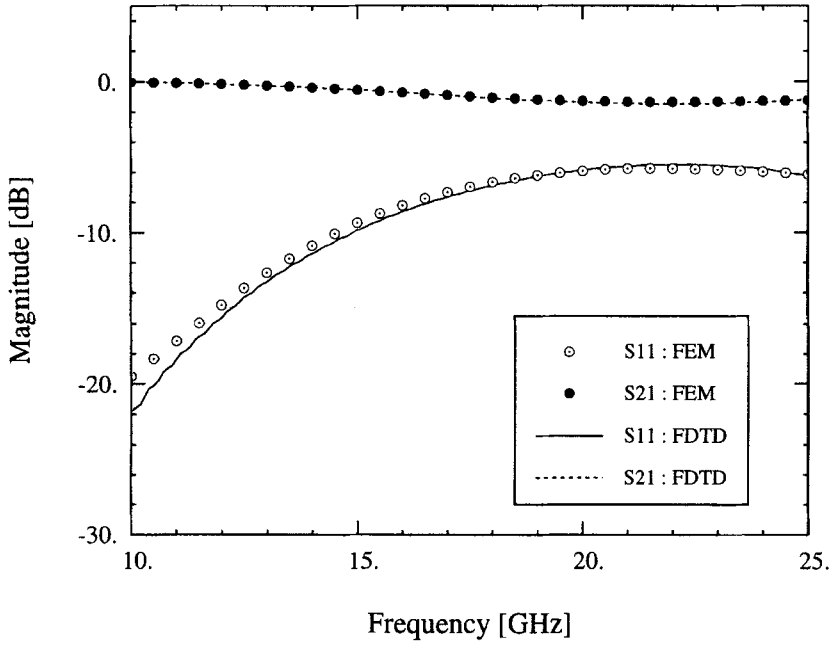

Figure 10. S-parameters of the extended rectangular via hole grounding case.

NUMERICAL RESULTS

Two different full-wave electromagnetic tools (FEM and FDTD) are applied throughout this article for the characterization of various transitions. In general, the FEM requires a multiple solution process for each frequency point, while the FDTD needs only one sweep in the time domain to give the whole frequency spectrum accurately. However, the FDTD demands finer discretization and requires greater computational cost than the FEM.

Microstrip-through-CPW Hermetic Transition

For an effective transition through a cavity wall, the microstrip line can be gradually changed into a coplanar waveguide which extends beyond each face of the hermetic wall as shown in Figure 1. The employed section of the coplanar waveguide is back metallized by the ground of the microstrip line and gives rise to parallel plate waveguide modes, parasitic radiation, and unwanted resonances that occur within the range of the operating frequencies. These resonances are pronounced when the structures are shielded, but are considerably damped when these transitions operate in an open environment.

To understand these effects, the hermetic transition is studied in several steps. At first, a simple microstrip-through-CPW transition, operating in open environment, is analyzed using FDTD and compared with experiments to understand the parasitic effects such as radiation and resonances introduced by the CPW section. The transition structure is then placed inside a closed cavity and characterized by using the FEM and the FDTD. Because the side walls can affect the performance of the circuit, one needs to be very careful in the choice of cavity width. In this article, to examine the effect of the cavity width, two different cavity sizes are considered without changing the other geometrical factors. In addition, vertical wires, rectangular via holes, extended via holes, and PEC walls are used to connect the CPW ground planes with the CPW backside metallization to eliminate the excited waveguide mode type resonances and the effects of these connections on the original circuit are investigated. By doing this, the effects of the resonances due to the cavity and the waveguide-like section under the CPW section are closely examined. Finally, a hermetic wall is introduced to complete the transition geometry.

Open Transition through a CPW Section. To quantify the performance of the CPW section utilized in the transition, the microstrip-through CPW planar transition in an open environment without via holes (see Fig. 1) is studied first. The method used for the theoretical modeling is the FDTD technique with appropriate boundary conditions to absorb radiation. The study in this section has revealed that the transition itself introduces a resonance around 17 GHz with a very low Q due to high parasitic radiation. Furthermore, the same structure is measured experimentally using the 8510 ANA and the Wiltron test fixture. The measurements are performed using a TRL de-embedding procedure and time domain gating is employed to suppress multiple reflections due to the finite substrate. As shown in Figure 2, the overall agreement between the FDTD and experimental results is satisfactory. The discrepancy observed in the higher frequency end of the spectrum is due to the structural difference between the modeled and measured geometries. Specifically, the FDTD approximated the exact geometrical factors of the transition to accommodate a uniform mesh and assumed an infinite substrate with the upper CPW ground and the lower conductor at

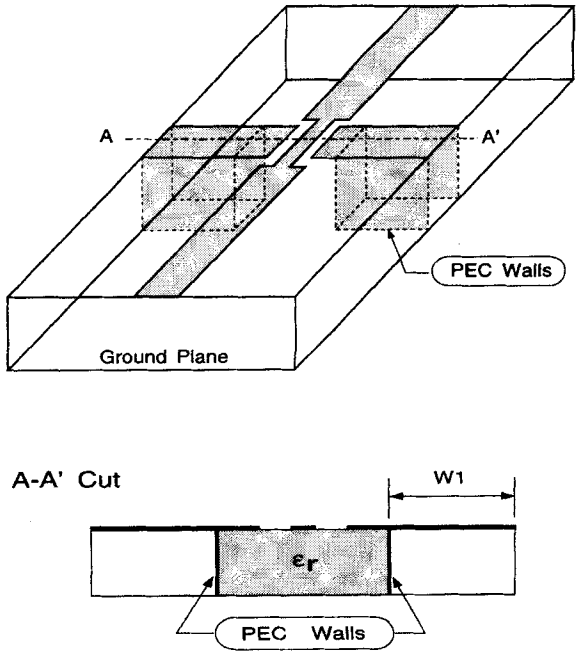

Figure 11. Geometry of the microstrip-through-CPW transition without hermetic wall: PEC wall grounding. W_1 = 2.034 mm and other geometric factors are identical to the first example.

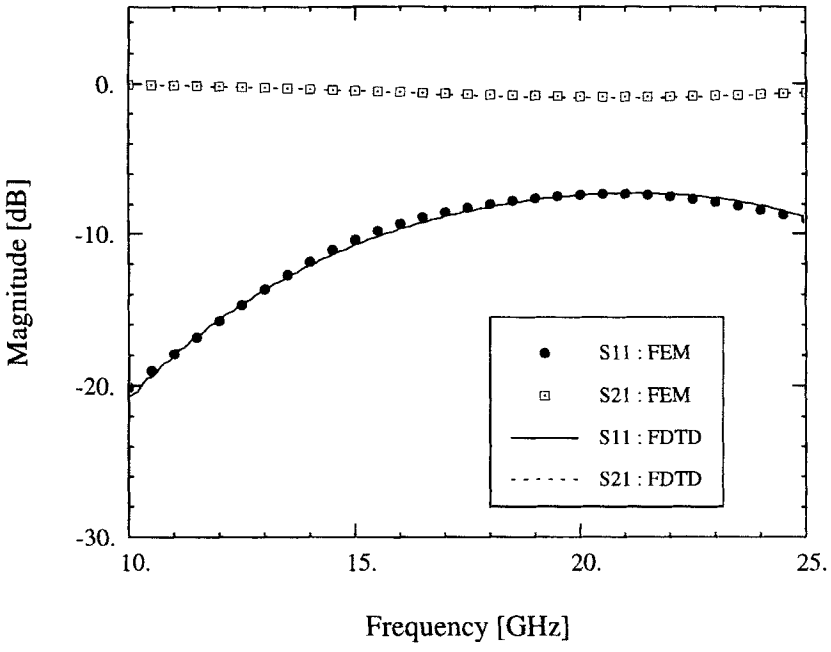

Figure 12. S-parameters of the PEC wall grounding case.

exactly the same potential. However, in the experiment we had to use finite-sized substrate and, even further, the CPW ground planes and lower conductor were connected using conducting strips to provide the same potential.

Closed Transition through a CPW Section. Following the treatment of the open transition, the same geometry is placed inside a metallic cavity and is characterized for two different cavity sizes. Figure 3 shows the computed S-parameters for $D = 2.26$ mm and 1.76 mm. As seen from the figures, the presence of the cavity, even though it is designed to be below cutoff at the frequencies of interest, drastically affects the performance by introducing high Q resonances. As expected [17–19], these resonances are shifted to higher frequencies as the cavity size decreases. For the case of $D = 2.26$ mm, there are two resonances in $|S_{21}|$ which are clearly observed at 21 GHz and around 9 GHz (not shown in the Fig. 3). These strong resonances are due to TE-like modes [38–40] excited in the region between the ground planes of the CPW section, its back metallization, and the side walls. Specifically, the resonance at 9 GHz corresponds to the TE_{10} mode of that waveguide-like section. The dips in $|S_{11}|$ around 15 GHz in Figure 3 are due to the length of the narrow microstrip line (W_5 in Fig. 1) as confirmed through another numerical experiment in Figure 4. That is, when the effective length of that section is

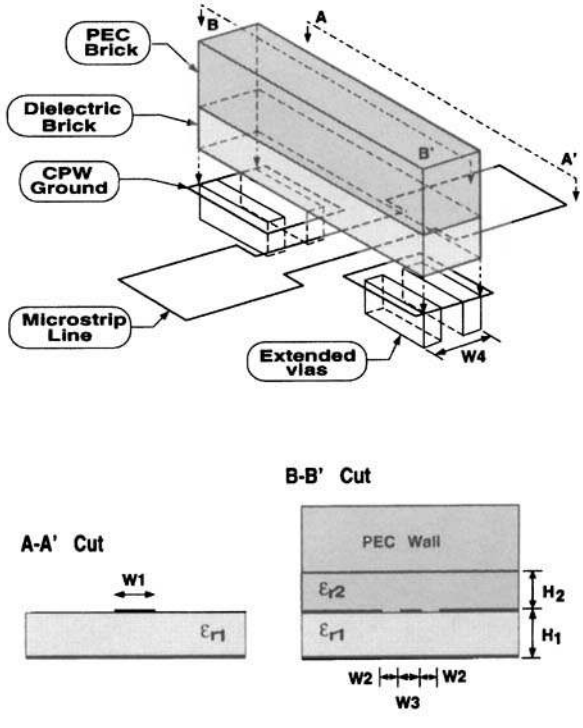

Figure 13. Geometry of the microstrip-through-CPW transition with hermetic wall on top of the extended PEC via grounding case. The width of the hermetic wall is 1.6 mm. $W_1 = 0.48$ mm, $W_2 = 0.14$ mm, $W_3 = 0.2$ mm, $W_4 = 1.6$ mm, $H_1 = H_2 = 0.635$ mm, $\epsilon_{r1} = 12.5$, $\epsilon_{r2} = 2.3$.

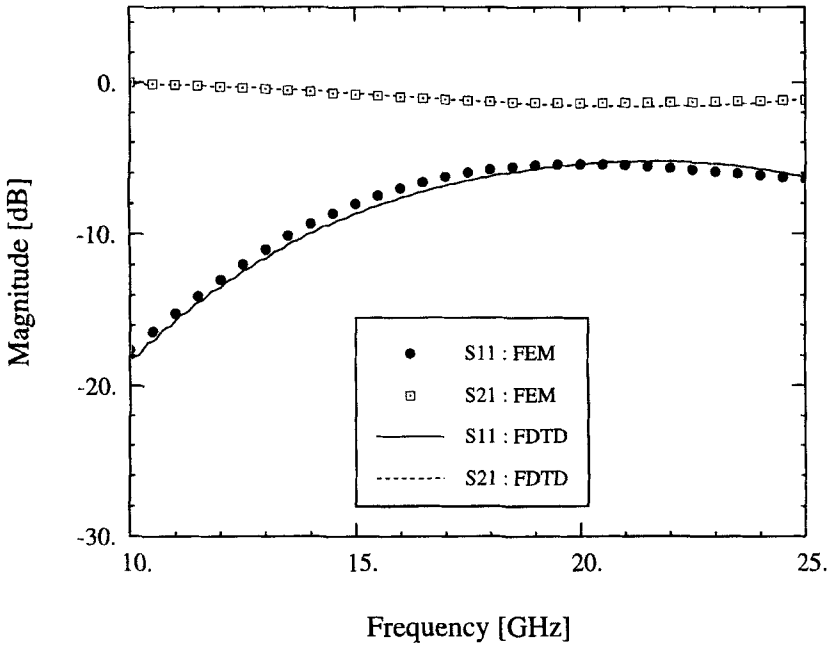

Figure 14. Comparison of the *S*-parameters for the transition with hermetic wall on top and extended PEC via under the circuit plane.

$\lambda_g/2$, total transmission can occur with the same input and output transmission lines as in our cases. Also, similar argument can be applied to the dips at 20 and 21 GHz in Figure 3 with the length of the CPW section. The return loss of case 1 is less than 10 dB in the frequency range of 11 to 20 GHz showing a good transition performance.

Theoretical data derived by the FEM and the FDTD method reveal the same resonances and

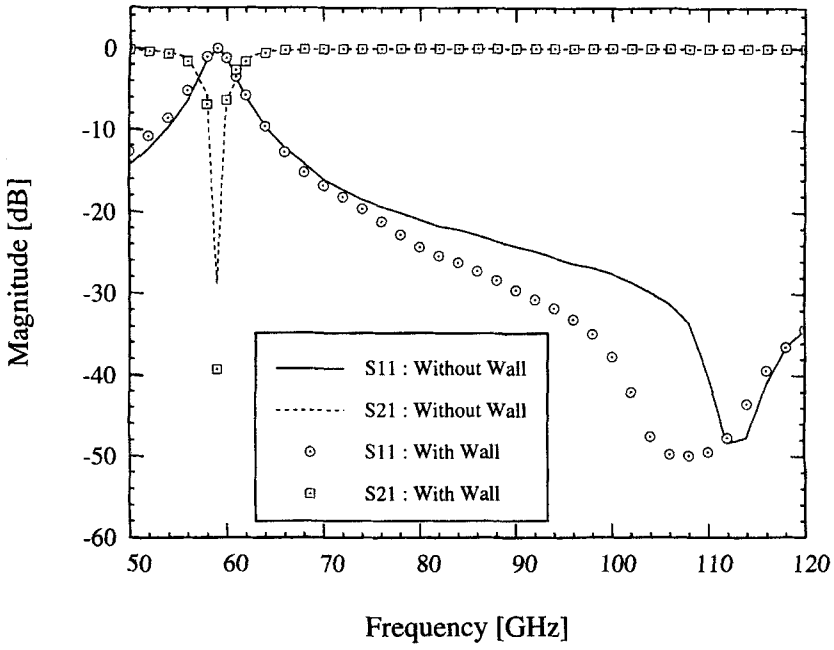

Figure 15. *S*-parameters for the transition with and without hermetic wall on top of the CPW section. Geometric factors: $W_1 = 70$ μm, $W_2 = 30$ μm, $W_3 = 40$ μm, $W_4 = 300$ μm, $W_5 = 350$ μm (refer to Fig. 2). The width and height of the dielectric brick under the PEC wall are 250 μm and 100 μm, respectively.

indicate the need for a mechanism to suppress them. The next subsections will be devoted to the investigation of a variety of mechanisms needed to suppress the excitation of the parasitic waveguide modes responsible for the previously observed resonances.

Vertical Wire Grounding. As a first attempt to eliminate the effect of the excited waveguide modes under the CPW section, vertical wires are used to connect the CPW ground planes and the PEC back-metallization under the substrate as shown in Figure 5. On either side of the longitudinal symmetry plane, four wires (400 μm apart) are inserted at a distance of 466 μm from the symmetry plane. These vertical wires are implemented as infinitely thin PEC wires for convenient numerical simulations.

Figure 6 shows the scattering parameters computed by both FEM and FDTD. The results shown in the figure indicate that, in the low frequency region (up to 13 GHz), the transition circuit performs fairly well, while it degrades as the operating frequency increases beyond 13 GHz. This degradation indicates that the wires play a role in increasing the resonance frequency, but do not suppress it completely. This is due to a waveguide-type resonance (TE_{10}-like mode) which develops between the wires and the side walls under the CPW section. They will always exist in some form as long as there is an enclosure.

Rectangular via Hole Grounding. In this subsection, rectangular PEC via holes are used to connect the CPW ground planes to the bottom PEC surface (see Fig. 7). There are four via holes and the size of each via hole is 600 × 452 μm and the

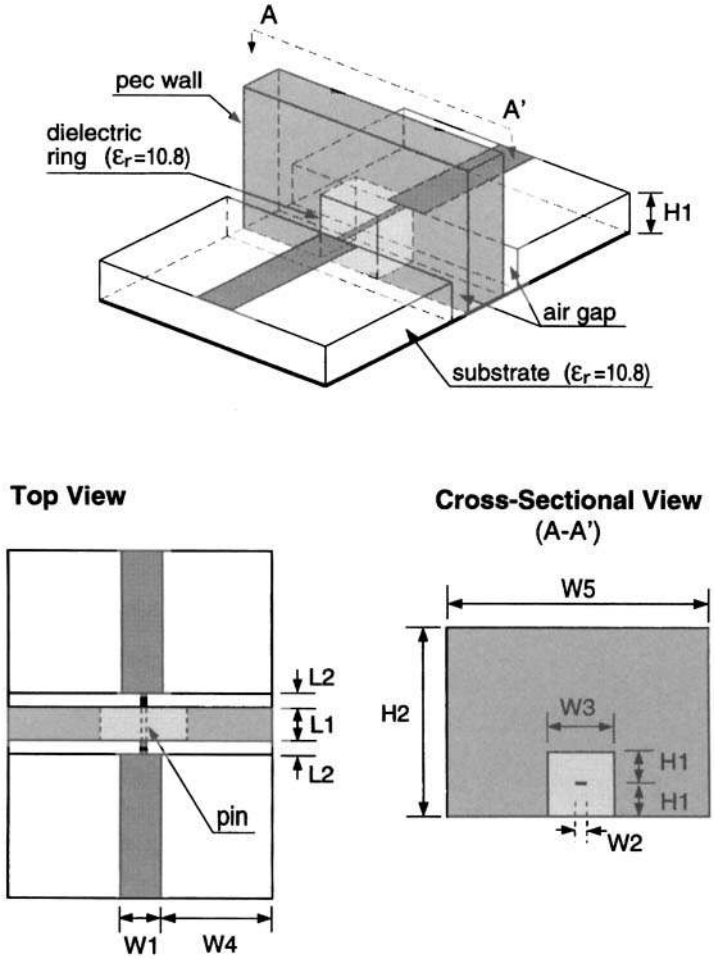

Figure 16. Geometry of the hermetic bead transition. W_1 = 0.55 mm, W_2 = 0.21 mm, W_3 = 1.27 mm, W_4 = 2.225 mm, W_5 = 5.0 mm, H_1 = 0.635 mm, H_2 = 4.0 mm, L_1 = 1.50 mm, L_2 = 0.40 mm, ϵ_r = 10.8.

height is 635 μm, which is the same as the substrate thickness. Also, the ground plane of the CPW is reduced to half of the original size.

The calculated S-parameters are shown in Figure 8. The overall frequency response of the structure is similar to the wire grounding case, but the resonant frequency is shifted to a further higher frequency region. This is due to the reduced distance ($W_3 + W_4 = 1.582$ mm in Fig. 7) between the PEC via walls and the cavity side walls. Note that the aforementioned waveguide-like structure has incomplete side and top walls, as shown in Figure 8, and this explains the reduced Q at the resonance of approximately 23 GHz.

Extended Rectangular via Hole Grounding. To avoid excitation of waveguide-like modes under the conductor-backed CPW section, extended via holes are placed under the CPW ground planes (see Fig. 9) and their effect is investigated. Analysis of this structure confirms that the extended rectangular via holes suppress unwanted resonances (Fig. 10). The field distribution around the transition region also verifies the suppression of the resonant field under the CPW ground pads. As shown in Figure 10, the overall return loss is improved by about 2 dB by extending the via holes while the performance of the transition structure degrades as frequency increases. Specifically, over 15 GHz, it has more than 10 dB return loss. The effect of the extended vias may be simulated by an array of vias.

PEC Wall Grounding. In this subsection, the effect of further extension of the via holes to form solid walls under the CPW ground pads is studied. The schematic view is shown in Figure 11. Figure 12 shows the computed frequency response of the transition with solid walls under the CPW ground pads. As expected, the transition characteristics are improved over the previous structure with extended via holes. After the PEC walls are inserted, the resonance phenomenon vanished and the S_{11} decreased. In particular, in the high frequency region, the circuit performance with the solid PEC wall is improved by 2 to 3 dB in return loss.

Up to this point, the effects of the cavity size, vertical wires, and various shapes of via holes which connect the CPW ground to the PEC surface under the substrate have been examined. In the next subsection, the effect of the hermetic wall on top of the circuit is studied.

Microstrip-through-CPW Transition with Hermetic Wall. In this subsection, the effect of the hermetic wall on the microstrip-through-CPW transition with extended vias is investigated. The hermetic wall is formed by a ceramic material bonded on top of a metal plate which forms the upper part of the wall. Figure 13 shows the geometrical details of the hermetic transition structure with extended via holes. The height of the ceramic is equal to the substrate thickness while its relative dielectric constant is chosen to be $\epsilon_{r2} = 2.3$, in contrast to the 12.5 of the substrate. From a

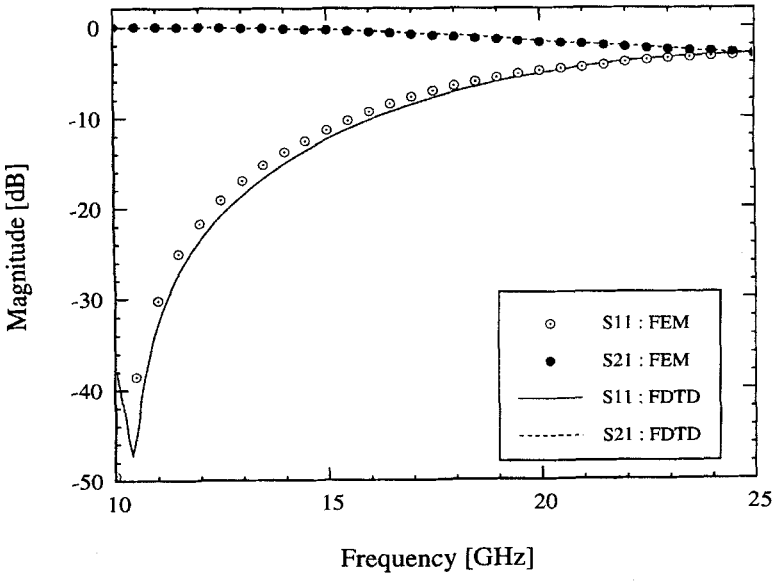

Figure 17. S-parameters of the hermetic bead transition with square dielectric ring.

circuits point of view, the ceramic on top of the transmission line may alter the characteristic impedance of the line, and hence it may affect the resulting S-parameters. Since there is a conducting plane on top of the ceramic, the CPW with hermetic wall can be considered as an inhomogeneously sandwiched CPW and its characteristic may be slightly affected.

In Figure 14, the magnitude of the scattering parameters obtained using FEM and FDTD are compared. After placing the hermetic wall on top of the CPW section, the overall return loss has

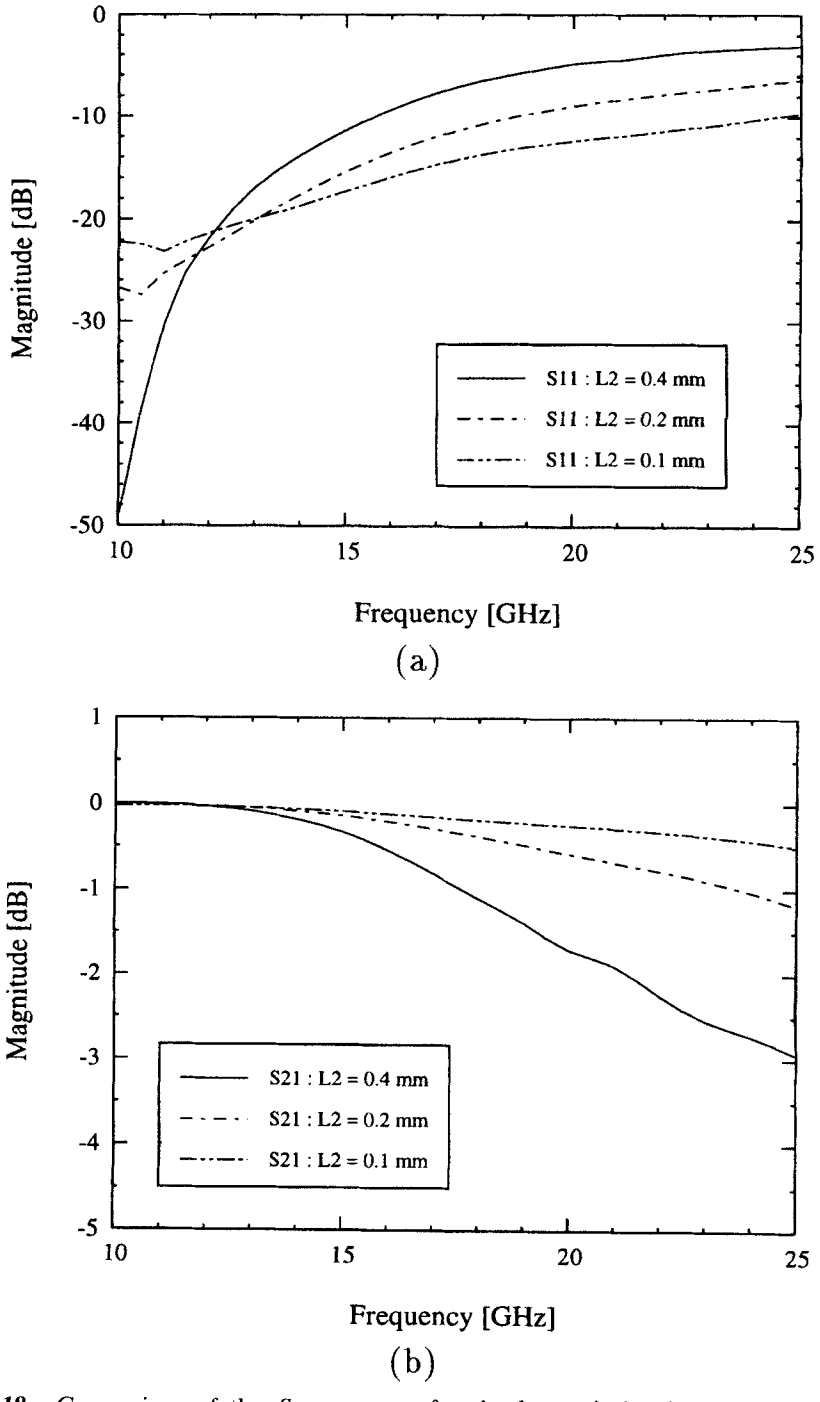

Figure 18. Comparison of the S-parameters for the hermetic bead transition of three different air gap widths of L_2. (a) $|S_{11}|$ and (b) $|S_{21}|$.

increased by 2 to 3 dB while its frequency dependency has remained unchanged. In the whole frequency region considered, from 10 to 25 GHz, the return loss is less than −5 dB. However, in the low end of this frequency region, up to 13 GHz, the return loss is less than −10 dB. The effect of the hermetic wall is small as expected from the field distribution in the CPW structure.

W-Band Application of the Hermetic Transition. Based on the previous results, a transition from the microstrip-through-CPW section has been designed to investigate the possibility of using the hermetic wall transition in the W-band application. The hermetic wall is built on top of the CPW section of the microstrip-through-CPW transition and the width and thickness are chosen to be 250 μm and 100 μm, respectively, with a dielectric constant of 2.5. The *S*-parameters computed in the shielded environment using the FEM are shown in Figure 15. It is observed that the transitions with and without the hermetic wall show very similar characteristics. In particular, in the high frequency region, over 70 GHz, the transition reveals very good performance, having less than −20 dB of return loss.

Interchip Transition: Hermetic Bead Transition

Square Dielectric Ring. Another type of commonly encountered feed-through, the hermetic bead transition structure, is analyzed in this subsection. As shown in Figure 16, a circular coaxial line is approximated with rectangular-shaped stripline and the dimensions are chosen to have 50-Ω characteristic impedance. Also, the dielectric constant of the ring is chosen as 10.8, which is the same as the substrate. The thickness of the hermetic wall and the air gap spacings are chosen as 1.5 mm and 0.4 mm, respectively.

S-parameters computed using FEM and FDTD are shown in Figure 17. The hermetic bead transition performs quite well in the low frequency end of the region, as expected, while the return loss degrades as frequency increases. To improve the performance of the transition and to provide useful design information, the air gap spacing (L_2) is varied from 0.4 mm to 0.1 mm. The computed *S*-parameters are shown in Figure 18 for three different cases. As we can observe, the overall transition performances are improved as the air gap spacing is decreased. Although the geometrical factors are not optimized for better transition characteristics, the overall performance of the circuit gives an essential understanding of the performance of this type of transition.

Circular Dielectric Ring. For an investigation of the effect of the rectangular approximation of a circular ring, the hermetic bead transition with circular dielectric ring is studied in this subsection. The radius of the circular ring is chosen as H_1 so that the circular ring is fit into the square

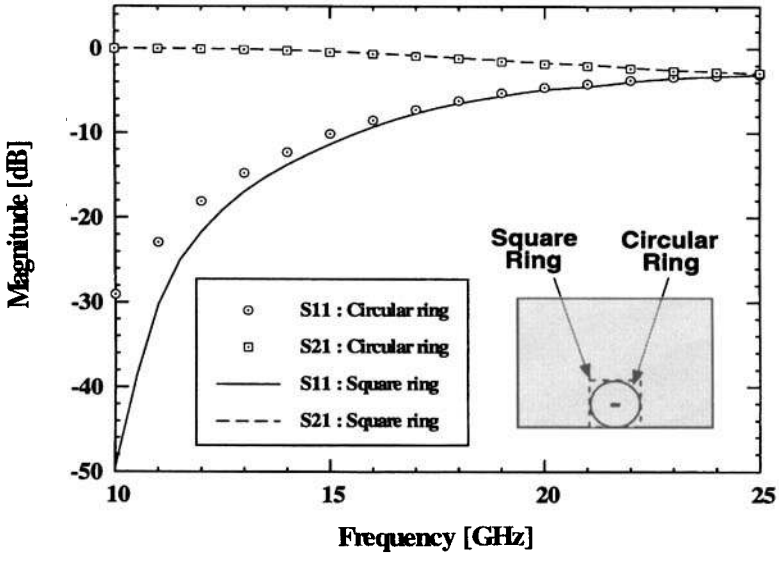

Figure 19. Comparison of the *S*-parameters of the hermetic bead transition with square and circular dielectric ring of radius H_1.

hole. As shown in Figure 19, the performance of the circular ring is very similar to that of the square one except at the lower frequency region. The degraded performance of the circular ring is mainly due to the effect of the conductor placed closer than the square one.

CONCLUSIONS

The finite element method (FEM) and the finite difference time domain (FDTD) technique have been used to characterize the effect of the hermetic walls commonly encountered in MIC and MMIC packaging. The derived FEM and FDTD results, as well as measurement, agreed very well in low as well as high frequency regions. It was shown that the grounding structures (wires, vias, and PEC walls), which are placed under the CPW ground pads to equalize the potential between the ground planes on the upper and lower surfaces, play a key role in the performance of this transition. The hermetic wall placed on top of the CPW transmission line section degrades the return loss of the original circuit only by a couple of decibels. In addition, a hermetic bead transition structure was designed and analyzed for the circular- and rectangular-shaped ring and the effect of air gap spacing was also studied. The performance of this transition was found to gradually degrade as frequency increased.

ACKNOWLEDGMENT

This research was supported by the U.S. Army Research Office and Texas Instruments.

REFERENCES

1. J. D. Montgomery, "Hybrid MIC North American Markets," *Microwave J.*, Vol. 32, April 1989, pp. 32–39.
2. H. Bierman, "Designers Strive for Low Cost MMIC Packages," *Microwave J.*, Vol. 35, Sept. 1992, pp. 100–106.
3. S. Joshi and B. Becker, "Metal Hermetic Surface Mount Packaging," *Microwave J.*, July 1992, Vol. 35, pp. 144–145.
4. B. Ziegner, "High Performance MMIC Hermetic Packaging," *Microwave J.*, Nov. 1986, Vol. 29, pp. 133–139.
5. D. Hughes and D. Jackson, "An Equivalent Circuit for a Microwave Surface Mount Package," *Microwave J.*, Vol. 34, Oct. 1991, pp. 134–144.
6. R. DeBoo, S. Hinderks, and N. Osbrink, "New Surface-Mounted Package Breaks from Traditional MIC Packaging," *Microwave J.*, Vol. 27, March 1984, pp. 126–134.
7. D. Hughes, H. Harris, and C. Rucker, "An Equivalent Circuit for a 70 mil Microstrip Package," *Microwave J.*, Vol. 27, Aug. 1986, pp. 97–102.
8. H. R. Malone, "Antenna/MMIC Packaging Techniques for Commercial Applications," *1992 IEEE Ant. Propagat. Soc. Int. Symp. Dig.*, Vol. 3, 1992, p. 1264.
9. L. Katehi, "The Role of EM Modeling in Integrated Packaging," *1993 IEEE Ant. Propagat. Soc. Int. Symp. Dig.*, Vol. 2, 1993, pp. 982–985.
10. D. S. Wein, "Advanced Ceramic Packaging for Microwave and Millimeter Wave Applications," *1993 IEEE Ant. Propagat. Soc. Int. Symp. Dig.*, Vol. 2, 1993, pp. 993–996.
11. H. Kuno, T. Milford, and J. Wooldridge, "The Evolution of MMIC Packaging," *1993 IEEE Ant. Propagat. Soc. Int. Symp. Dig.*, Vol. 2, 1993, pp. 1013–1016.
12. M. Ida and T. Nishikawa, "A Multilayered Package Technology for MMICs," *1993 IEEE Ant. Propagat. Soc. Int. Symp. Dig.*, Vol. 2, 1993, pp. 1005–1007.
13. D. Griffin, "A New Instrument and Technique for Diagnosing Electromagnetic Design Problems in Microwave Module Housings and Component Packages," *IEEE Trans. Instrumentat. Meas.*, Vol. 41, Feb. 1992, pp. 27–31.
14. L. Lu, C. Wu, and J. Litva, "A New 3D-FDTD Simulator for Modeling Electronic Interconnections and Packaging," *Proceedings of the IEEE 2nd Topical Meeting on Electrical Performance of Electronic Packaging*, pp. 92–95.
15. IEEE 2nd Topical Meeting on Electrical Performance of Electronic Packaging, Monterey, California, Oct. 1993.
16. W. D. Becker, P. H. Harms, and R. Mittra, "Time-Domain Electromagnetic Analysis of Interconnects in a Computer Chip Package," *IEEE Trans. Microwave Theory Tech.*, Vol. MTT-40, Dec. 1992, pp. 2155–2163.
17. L. Dunleavy and P. Katehi, "Shielding Effects in Microstrip Discontinuities," *IEEE Trans. Microwave Theory Tech.*, Vol. 36, Dec. 1988, pp. 1767–1774.
18. L. Wu and Y. Chang, "Characterization of the Shielding Effects on the Frequency-Dependent Effective Dielectric Constant of a Waveguide-Shielded Microstrip Using the Finite-Difference Time-Domain Method," *IEEE Trans. Microwave Theory Tech.*, Vol. 36, Oct. 1991, pp. 1688–1693.
19. C. Amrani, M. Drissi, V. Fouad, and J. Citerne, "Packaging and Interconnection Mutual Coupling Effects in Planar Structures and Discontinuities," *1993 IEEE Int. MTT-S Symp. Dig.*, 1994, pp. 843–846.

20. P. Mezzanotte, M. Mongiardo, L. Roselli, and R. Sorrentino, "FDTD Analysis of High Performance MMIC Package," *1994 IEEE Int. MTT-S Symp. Dig.*, 1994, pp. 337–340.
21. G. Strauss and W. Menzel, "A Novel Concept for MM-Wave MMIC Interconnects and Packaging," *1994 IEEE Int. MTT-S Symp. Dig.*, 1994, pp. 1141–1144.
22. R. Faraji-Dana and Y. Chow, "A CAD Tool for Interference Rejection of a Microwave Circuit Making Use of Response of the Circuit Packaging," *1994 IEEE Int. MTT-S Symp. Dig.*, 1994, pp. 1523–1526.
23. M. Tsuji and H. Shigesawa, "Packaging of Printed-Circuit Lines: A Dangerous Cause for Narrow Pulse Distortion," *IEEE Trans. Microwave Theory Tech.*, Vol. 42, Sept. 1994, pp. 1784–1790.
24. P. Mezzanotte, M. Mongiardo, L. Roselli, R. Sorrentino, and W. Heinrich, "Analysis of Packaged Microwave Integrated Circuits by FDTD," *IEEE Trans. Microwave Theory Tech.*, Vol. 42, Sept. 1994, pp. 1796–1801.
25. R. Goyal, "Designing A 100 MHZ SPARC Dual Processor Using MCM-L Packaging Technology and Microwave Design Techniques," *1994 IEEE Int. MTT-S Symp. Dig.*, 1994, pp. 1715–1718.
26. M. Rittweger, M. Werthen, and I. Wolff, "3D FDTD Analysis Applied to the Investigation of the Resonant Behavior of Ceramic Feedthrus," *1994 IEEE Int. MTT-S Symp. Dig.*, 1994, pp. 1719–1722.
27. T. Shibata, S. Kimura, H. Kimura, Y. Imai, Y. Umeda, and Y. Akazawa, "Design Technique for a 60-GHz-Bandwidth Distributed Baseband and Amplifier IC Mudule," *IEEE J. Solid-State Circ.*, Vol. 29, Dec. 1994, pp. 1537–1544.
28. M. L. Barton and Z. J. Cendes, "New Vector Finite Elements for Three-Dimensional Magnetic Field Computation," *J. Appl. Phys.*, Vol. 61, No. 8, April 1987, pp. 3919–3921.
29. J-G. Yook, N. I. Dib, and L. Katehi, "Characterization of High Frequency Interconnects Using Finite Difference Time Domain and Finite Element Methods," *IEEE Trans. Microwave Theory Tech.*, Vol. 42, Sept. 1994, pp. 1727–1736.
30. J.-Fa Lee, "Analysis of Passive Microwave Devices by using Three-Dimensional Tangential Vector Finite Elements," *Int. J. Num. Model. Electron. Net. Dev. Fields*, Vol. 3, 1990, pp. 235–246.
31. W. Schroeder and Ingo Wolff, "The Origin of Spurious Modes in Numerical Solutions of Electromagnetic Field Eigenvalue Problems," *IEEE Trans. Microwave Theory Tech.*, Vol. 42, April 1994, pp. 644–653.
32. T. K. Sarkar and E. Arvas, "On a Class of Finite Step Iterative Methods (Conjugate Directions) for the Solution of an Operator Equation Arising in Electromagnetics," *IEEE Trans. Ant. Propagat.*, Vol. AP-33, Oct. 1985, pp. 1058–1066.
33. K. Kunz and R. Luebbers, *The Finite Difference Time Domain Method for Electromagnetics*. CRC Press, Boca Raton, FL, 1993.
34. X. Zhang and K. Mei, "Time-Domain Finite Difference Approach to the Calculation of the Frequency-Dependent Characteristics of Microstrip Discontinuities," *IEEE Trans. Microwave Theory Tech.*, Vol. 36, Dec. 1988, pp. 1775–1787.
35. D. Sheen, S. Ali, M. Abouzahra, and J. Kong, "Application of the Three-Dimensional Finite-Difference Time-Domain Method to the Analysis of Planar Microstrip Circuits," *IEEE Trans. Microwave Theory Tech.*, Vol. 38, July 1990, pp. 849–857.
36. T. Shibata and H. Kimura. "Computer-Aided Engineering for Microwave and Millimeter-Wave Circuits Using the FD-TD Technique of Field Simulations," *Int. J. MIMICAE*, Vol. 3, No. 3, 1993, pp. 238–250.
37. A. Engel, N. Dib, and L. Katehi, "Characterization of a Shielded Transition to a Dielectric Waveguide," *IEEE Trans. Microwave Theory Tech.*, Vol. 42, May 1994, pp. 847–854.
38. Ke Wu, R. Vahldieck, J. L. Fikart, and H. Minkus, "The Influence of Finite Conductor Thickness and Conducitivity on Fundamental and Higher-Order Modes in Miniature Hybrid MIC's (MHMIC's) and MMIC's" *IEEE Trans. Microwave Theory Tech.*, Vol. 41, March 1993, pp. 421–430.
39. Ming Yu, R. Vahldieck, and Ke Wu, "Theoretical and Experimental Characterization of Coplanar Waveguide Discontinuities," *IEEE Trans. Microwave Theory Tech.*, Vol. 41, Sept. 1993, pp. 1638–1640.
40. M. Yu, R. Vahldieck, and J. Huang. "Comparing Coax Launcher and Wafer Probe Excitation for 10 mil Conductor Backed CPW with Via Holes and Airbridges," *1993 IEEE MTT-S Int. Microwave Symp. Dig.*, pp. 705–708.

BIOGRAPHIES

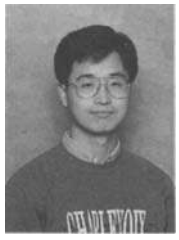

Jong-Gwan Yook (S'86) was born in Korea, in 1964. He received the BS and MS degrees in electronic engineering from Yonsei University, Seoul, Korea, in 1987 and 1989, respectively. He is currently working toward the PhD degree in electrical engineering at the University of Michigan, Ann Arbor, as a graduate student research assistant in the Radiation Laboratory. His main research interests are in the area of electromagnetic characterization of VLSI and MMIC interconnects using the finite element method and development of numerical techniques for analysis and design of high frequency circuits with emphasis on parallel computing.

Nihad I. Dib received the BSc and MSc degrees in electrical engineering from Kuwait University, in 1985 and 1987, respectively, and the PhD degree in electrical engineering from the University of Michigan, Ann Arbor, in 1992. From 1993 to 1995, he was an assistant research scientist at the Radiation Laboratory, University of Michigan. In September 1995, he joined the Electrical Engineering Department at the Jordan University of Science and Technology as an assistant professor. His research interests include the numerical analysis and modeling of planar discontinuities and dielectric lines.

Eray Yasan was born in Samsun, Turkey, in 1968. He received his BS degree in electrical and electronics engineering from Hacettepe University in 1990 and his MS degree in electrical engineering from the University of Michigan in 1995. He had worked a teaching assistant for microwaves courses in the Electrical Electronics Engineering Department of Hacettepe University until mid-1993. Meanwhile, he was involved in analysis of mutual coupling effects of rectangular microstrip patch antennas. He is now studying toward his PhD in electrical engineering at the University of Michigan. His current research interests include analysis of microwave circuits with lumped passive and active elements using FEM (finite element method).

For **Linda P. B. Katehi**'s biography and photo, please see page 296.